

Simultaneous Prediction of Muscle and Contact Forces in the Knee during Gait

Yi-Chung Lin^a, Jonathan P. Walter^a, Scott A. Banks^a, Marcus G. Pandy^b, and

Benjamin J. Fregly^{a,b,c,d}

^aDept. of Mechanical & Aerospace Engineering, University of Florida, Gainesville, FL, USA

^bDept. of Mechanical Engineering, University of Melbourne, Melbourne, Australia

^cDept. of Biomedical Engineering, University of Florida, Gainesville, FL, USA

^dDept. of Orthopaedics and Rehabilitation, University of Florida, Gainesville, FL, USA

Revised manuscript submitted as an original article to the

Journal of Biomechanics

October 4, 2009

Corresponding author: B.J. Fregly, Ph.D.

Department of Mechanical & Aerospace Engineering

231 MAE-A Building

P.O. Box 116250

University of Florida

Gainesville, FL 32611-6250

Phone: +1-352-392-8157

Fax: +1-352-392-7303

E-mail: fregly@ufl.edu

Keywords: Musculoskeletal model; muscle force; contact force; inverse dynamic optimization.

Word count: 3,764

Abstract

1
2 Musculoskeletal models are currently the primary means for estimating *in vivo* muscle and
3 contact forces in the knee during gait. These models typically couple a dynamic skeletal model
4 with individual muscle models but rarely include articular contact models due to their high
5 computational cost. This study evaluates a novel method for predicting muscle and contact forces
6 simultaneously in the knee during gait. The method utilizes a 12 degree-of-freedom knee model
7 (femur, tibia, and patella) combining muscle, articular contact, and dynamic skeletal models.
8 Eight static optimization problems were formulated using two cost functions (one based on
9 muscle activations and one based on contact forces) and four constraints sets (each composed of
10 different combinations of inverse dynamic loads). The estimated muscle and contact forces were
11 evaluated using *in vivo* tibial contact force data collected from a patient with a force-measuring
12 knee implant. When the eight optimization problems were solved with added constraints to
13 match the *in vivo* contact force measurements, root-mean-square errors in predicted contact
14 forces were less than 10 N. Furthermore, muscle and patellar contact forces predicted by the two
15 cost functions became more similar as more inverse dynamic loads were used as constraints.
16 When the contact force constraints were removed, estimated medial contact forces were similar
17 and lateral contact forces lower in magnitude compared to measured contact forces, with
18 estimated muscle forces being sensitive and estimated patellar contact forces relatively
19 insensitive to the choice of cost function and constraint set. These results suggest that
20 optimization problem formulation coupled with knee model complexity can significantly affect
21 predicted muscle and contact forces in the knee during gait. Further research using a complete
22 lower limb model is needed to assess the importance of this finding to the muscle and contact
23 force estimation process.

1 **1. Introduction**

2 When the human musculoskeletal system is impaired, mobility is often limited, leading to a
3 decreased quality of life (Praemer et al., 1999). Common clinical examples include osteoarthritis,
4 patellofemoral pain, stroke, cerebral palsy, and paraplegia. Knowledge of *in vivo* muscle and
5 joint contact forces during normal and pathological walking would assist clinicians in diagnosing
6 musculoskeletal disorders and developing new or improved treatments. Since direct
7 measurement of these internal forces is not clinically feasible, musculoskeletal modeling has
8 become the primary approach for developing estimates (Anderson and Pandy, 2003; Neptune et
9 al., 2004; Buchanan et al., 2005; Jinha et al., 2006; Shelburne et al., 2006; Liu et al., 2008; Besier
10 et al., 2009). However, because of the “muscle redundancy problem” (i.e., more muscles than
11 degrees of freedom in the skeletal model) (Crowninshield, 1978), estimates of *in vivo* muscle and
12 contact forces during gait remain largely unvalidated, particularly for the knee where multiple
13 bones articulate over multiple surfaces.

14 Recent *in vivo* contact force measurements made with instrumented knee implants provide an
15 opportunity for quantitative evaluation of muscle and contact force estimates during gait
16 (Kaufman et al., 1996; Taylor et al., 2004; D'Lima et al., 2005a; D'Lima et al., 2005b; D'Lima et
17 al., 2006). Since muscle forces are the primary determinants of joint contact forces (Anderson
18 and Pandy, 2003; Herzog et al., 2003; Shelburne et al., 2004), accurate estimates of joint contact
19 forces would imply reasonable estimates of muscle forces. To date, musculoskeletal modeling
20 studies that estimated *in vivo* tibial contact forces during gait have used a sequential (or
21 two-stage) computational approach (Taylor et al., 2004; Shelburne et al., 2005; Kim et al., 2009).
22 In the first stage, muscle forces were estimated using a musculoskeletal model without articular
23 contact, where muscle redundancy was resolved using inverse dynamic (i.e., static) or forward
24 dynamic optimization. In the second stage, contact forces were estimated by applying the

Revision 1

1 estimated muscle forces to a separate articular contact model (Kim et al., 2009) or static
2 equilibrium model in the superior-inferior direction (Taylor et al., 2004; Shelburne et al., 2005).
3 Articular contact models were omitted in the first stage presumably due to their high
4 computational cost and complexity (Bei and Fregly, 2004).

5 This sequential approach possesses three important limitations, all of which stem from the
6 lack of an articular contact model in the first stage. First, it does not utilize all available inverse
7 dynamic loads as constraints when static optimization is used. Of the six inverse dynamic loads
8 acting on the tibia, only those to which contact forces are assumed not to contribute can be used
9 as constraints. Usually only the net flexion-extension torque is assumed to fulfill this requirement
10 (e.g., Anderson and Pandy, 2001), and consequently the feasible solution space is not narrowed
11 to the fullest extent possible. Second, it assumes that contact forces do not affect muscle forces
12 (though muscle forces are assumed to affect contact forces). Though one study has proposed
13 minimization of compressive contact forces for muscle force estimation (Schultz and Andersson,
14 1981), such a criterion cannot be investigated using the sequential approach. Third, it requires
15 assumptions about patellar motion in the first stage. These assumptions may be inconsistent with
16 the patellar motion (and hence quadriceps moment arms) predicted in the second stage, thereby
17 affecting the estimated muscle and contact forces.

18 This study takes a fundamentally different approach by estimating muscle and contact forces
19 *simultaneously* in the knee during gait. A single three-dimensional knee model combining
20 muscle, articular contact, and dynamic skeletal models is used to develop the estimates. Two
21 contacts (medial and lateral) are modeled for the tibiofemoral (TF) joint and one contact for the
22 patellofemoral (PF) joint. The high computational cost and complexity of articular contact
23 models is eliminated by using “fast” surrogate contact modeling techniques (Lin et al., 2006; Lin
24 et al., 2008; Lin et al., 2009). Muscle redundancy is resolved using static optimization with two

Revision 1

1 cost functions and four constraint sets to investigate how optimization problem formulation
2 affects the calculated muscle and contact forces. Medial and lateral contact force estimates are
3 evaluated quantitatively using *in vivo* tibial contact force measurements obtained from the same
4 subject (Zhao et al., 2007a). Our hypotheses were that the model would be able to reproduce all
5 available *in vivo* contact force and inverse dynamic data simultaneously and that muscle and
6 contact forces estimated by the two cost functions would become more similar as more inverse
7 dynamic loads were used as constraints.

8

9 **2. Methods**

10 *2.1 Experimental Data Collection*

11 Previously reported experimental gait data collected from an adult male subject implanted
12 with an instrumented knee replacement (age 80, mass 68 kg, height 1.7 m, right knee, neutral
13 alignment) eight months after surgery were used for this study (Zhao et al., 2007a; Zhao et al.,
14 2007b). Institutional review board approval and patient informed consent were obtained.

15 The subject performed two types of gait tasks. The first type was treadmill gait under
16 fluoroscopic motion analysis and the second was overground gait under video motion analysis
17 (Motion Analysis Corporation, Santa Rosa, CA) with simultaneous collection of ground reaction
18 data (AMTI Corporation, Watertown, MA). Instrumented knee data were collected
19 simultaneously in both cases. One overground gait trial with cadence closest to the fluoroscopic
20 gait data was selected for subsequent analysis, as one trial was found to be sufficient for
21 demonstrating differences due to optimization problem formulation. Further details on the
22 experimental data collection can be found in Zhao et al. (2007a,b).

23 The subject was implanted with a first-generation instrumented knee design (D'Lima et al.,
24 2005b). The implant consisted of four uniaxial force transducers, a micro transmitter, and an

Revision 1

1 antenna. The distribution of contact forces between the medial and lateral compartments was
2 calculated from the four force transducer measurements using validated regression equations
3 (Zhao et al., 2007a). Further details on the instrumented implant design can be found in D’Lima
4 et al. (2005b).

5

6 *2.2. Musculoskeletal Model Development*

7 A 12 degree-of-freedom (DOF) patient-specific knee model actuated by eleven muscles and
8 possessing TF and PF articular contact (Fig. 1) was constructed to calculate muscle and contact
9 forces simultaneously for the instrumented knee. The femur in the knee model was fixed to
10 ground, while the tibia and patella were allowed to move relative to the femur via two separate 6
11 DOF joints (i.e., 3 translations and 3 rotations). The equations of motion for the model were
12 derived using Autolev symbolic manipulation software (OnLine Dynamics, Sunnyvale, CA).
13 Three-dimensional tibiofemoral and patellofemoral contact models were constructed using “fast”
14 surrogate contact modeling techniques (Lin et al., 2006; Lin et al., 2008; Lin et al., 2009). These
15 models reproduced 6 DOF load-displacement relationships sampled from elastic foundation (EF)
16 contact models of the subject’s implant components created from three-dimensional CAD
17 geometry with linear elastic material properties (Bei and Fregly, 2004). The complete knee
18 model was implemented in Matlab (The Mathworks, Natick, MA).

19 The eleven muscles included in the model were as follows: vastus medialis (VM), vastus
20 lateralis (VL), vastus intermedius (VI), rectus femoris (RF), semimembranosus (SM),
21 semitendinosus (ST), biceps femoris long head (BFLH), biceps femoris short head (BFSH),
22 tensor fascia latae (TFL), gastrocnemius medial head (GM), and gastrocnemius lateral head
23 (GL). Based on Anderson and Pandy (2001), the force generated by each muscle was modeled as
24 an activation times a peak isometric strength, where strength values were taken from Kim et al.

Revision 1

1 (2009). Each muscle was activated independently except for medial hamstrings (same activation
2 signal for SM and ST) and vasti (same activation signal for VM, VI, and VL), resulting in eight
3 activation signals. The patellar ligament was represented by three parallel linear springs with a
4 total stiffness of 2000 N/mm (Reeves et al., 2003). Other knee ligaments were not included in the
5 model.

6 Construction of the 12 DOF knee model involved registering a patient-specific inverse
7 dynamic skeletal model to a patient-specific geometric implant/bone model. The geometric
8 model was constructed from the patient's post-surgery CT data, CAD models of the patient's
9 implant components, and MR-derived bone models from a different subject of comparable
10 stature (Banks et al., 2005; Kim et al., 2009) (Fig. 2). This model provided muscle and patellar
11 ligament origin and insertion locations along with implant component locations within the bones.
12 The inverse dynamic model was constructed using the patient's overground gait data and
13 additional isolated joint motion trials processed within established patient-specific model
14 creation software (Reinbolt et al., 2005; Reinbolt et al., 2008). This model provided net loads
15 (i.e., three forces and three torques) acting on the instrumented tibia during overground gait. The
16 thigh and shank in the inverse dynamic model were registered to the femur and tibia/fibula in the
17 geometric model by finding the best-fit alignment between corresponding joint centers (ankle,
18 knee, and hip) and two additional points on corresponding knee functional axes (Fig. 3). The
19 functional axis for the geometric model was determined from the fluoroscopic motion data and
20 for the inverse dynamic model from the video motion data.

21 Additional details on Musculoskeletal Model Development can be found in the
22 Supplementary Material section.

23

Revision 1

1 *2.3 Muscle and Contact Force Estimation*

2 The 12 DOF patient-specific knee model was used to estimate muscle and contact forces
3 simultaneously using a two-level optimization approach. For each time frame during the gait
4 cycle, an outer-level muscle force optimization modified design variables related to muscle
5 activations while an inner-level pose optimization modified design variables related to tibial and
6 patellar pose on the femur. Given the current guess at the muscle activations, the inner-level
7 optimization found the resulting static configuration and returned the cost function and
8 constraints required by the outer-level optimization. Both optimizations were performed using a
9 Matlab nonlinear least-squares algorithm, with constraints being treated as penalty terms in an
10 augmented cost function so that inability to meet them would not cause the optimization
11 algorithm to fail.

12 The outer-level optimization used two cost functions and four constraint sets to investigate
13 how optimization problem formulation affects the calculated muscle and contact forces ([Glitsch](#)
14 [and Baumann, 1997](#); [Jinha et al., 2006](#)). The two cost functions were minimization of the sum of
15 the squares of muscle activations ([Kaufman et al., 1991](#); [Anderson and Pandy, 2001](#)) and
16 minimization of the sum of the three compressive contact forces (medial tibiofemoral, lateral
17 tibiofemoral, and patellofemoral) ([Schultz and Andersson, 1981](#)), where the direction of
18 compressive contact force was perpendicular to the planar back surface of the tibial insert or
19 patellar button. The four constraint sets were composed of different combinations of three
20 residual loads acting on the tibia (Table 1). Residual loads represent the differences between the
21 calculated inverse dynamic loads and the loads produced by the combined effect of muscle,
22 contact, and ligament forces. The remaining three residual loads acting on the tibia along with all
23 six residual loads acting on the patella were minimized as part of the inner-level pose
24 optimization.

Revision 1

1 The eight outer-level optimization problem formulations were solved two ways – with and
2 without additional constraints to match the *in vivo* medial and lateral contact force
3 measurements. Problems that included these constraints were termed “matched” formulations
4 and were used to verify that muscle forces in the model spanned the solution space necessary to
5 reproduce the *in vivo* contact force data. Problems that omitted these constraints were termed
6 “predicted” formulations and were used to evaluate how well different optimization problems
7 could predict the *in vivo* contact forces without knowing them a priori. One “matched”
8 formulation (minimize sum of squares of muscle activations using constraint set 1) was used to
9 verify that the muscle and contact force estimates generated using surrogate contact models
10 matched those generated using the EF contact models from which the surrogate contact models
11 were constructed. All optimization solutions were generated at 5% intervals throughout the gait
12 cycle.

13 Additional details on Muscle and Contact Force Estimation can be found in the
14 Supplementary Material section.

15

16 **3. Results**

17 Optimizations performed using the surrogate and EF contact models produced nearly
18 identical motion, contact force, and muscle force results, as demonstrated by the one selected
19 “matched” formulation. For the TF and PF joints, root-mean-square (RMS) differences in joint
20 translations/rotations and contact forces/torques were less than 0.6 mm/0.7 deg and 4 N/0.3 Nm,
21 respectively. Furthermore, both types of contact models reproduced the *in vivo* medial and lateral
22 contact force measurements accurately, with RMS errors being less than 10 N. RMS differences
23 in muscle force estimates generated by the two types of contact models were less than 15 N.
24 While approximately 90 minutes (32 hours) of CPU time were required to optimize one time

Revision 1

1 frame (one complete gait cycle) using the EF contact models, only 2 minutes (42 minutes) were
2 required when using the surrogate models.

3 The eight “matched” formulations accurately matched the *in vivo* medial and lateral contact
4 force measurements while producing different muscle force estimates depending on the selected
5 outer-level cost function and constraint set (Fig. 4 and 5). For all eight formulations, RMS errors
6 between measured and predicted contact forces were on the order of 10 N, and worst-case RMS
7 residual loads for the TF and PF joints were below 3 N and 1 Nm. The only exceptions were
8 constraint sets 2 and 4, where RMS residual loads for anterior-posterior force were on the order
9 of 100 N (see Supplementary Material). Unlike muscle forces, PF contact forces exhibited
10 similar magnitudes and shapes for all eight problem formulations with a maximum force of
11 approximately 250 N. RMS differences in muscle forces (PF contact forces) predicted by the two
12 cost functions decreased as more inverse dynamic loads were added as constraints (Table 2 –
13 top). None of the muscles exceed its maximum isometric force except for BFSH and TFL.

14 The eight “predicted” formulations predicted medial tibial contact forces that were
15 comparable and lateral tibial contact forces that were lower in magnitude compared to measured
16 tibial contact forces (Fig. 6). Larger lateral contact forces were generated when more inverse
17 dynamic loads than just the flexion-extension torque were used as constraints. One problem
18 formulation (minimize sum of three compressive contact forces using constraint set 2) predicted
19 the two *in vivo* peaks in medial and lateral contact force to within 29 N. Similar to the “matched”
20 solutions, muscle forces exhibited large changes and PF contact forces small changes when the
21 problem formulation was changed, with BFSH and TFL again being the only muscles to exceed
22 their maximum isometric forces (Fig. 7). While PF contact forces were similar to the “matched”
23 solutions, muscle forces exhibited noticeable differences in shape and magnitude (e.g., compare
24 “predicted” and “matched” solutions for TFL, MGAS, and LGAS). In contrast to the “matched”

Revision 1

1 solutions, RMS differences in muscle and PF contact forces predicted by the two cost functions
2 did not decrease as more inverse dynamic loads were added as constraints, nor did RMS
3 differences in medial and lateral contact forces (Table 2 – bottom).
4

5 **4. Discussion**

6 This study predicted muscle and contact forces simultaneously in the knee during gait using a
7 knee model that combined muscle, articular contact, and dynamic skeletal models. To our
8 knowledge, no previous study has included explicit articular contact models in the *in vivo* muscle
9 force estimation process for the knee. Inclusion of contact models allowed us to eliminate
10 assumptions about which inverse dynamic loads have little contribution from contact forces and
11 to investigate cost functions utilizing tibiofemoral and patellofemoral contact forces. Muscle
12 force estimates tended to be more sensitive to optimization problem formulation than were
13 contact force estimates, with PF contact force being especially insensitive. These observations
14 support the statement by Jinha et al. (2006) that “precise geometric representation of the
15 musculoskeletal system [is needed] if general force-sharing rules are to be derived.”

16 The simultaneous approach to muscle and contact force prediction used in this study was
17 made possible by our recent development of surrogate contact modeling methods (Lin et al.,
18 2006; Lin et al., 2008; Lin et al., 2009). While it is theoretically possible to employ EF contact
19 models for the simultaneous approach, as demonstrated by the one selected “matched”
20 formulation, 32 hours of CPU time per optimization is undesirable for performing repeated
21 optimizations with different problem formulations. Though the computational cost of
22 constructing the three surrogate contact models was on the order of 30 hours of CPU time, this
23 cost was paid once initially and then quickly redeemed by the 42 minutes of CPU time required
24 to solve the optimization problem over one full gait cycle.

Revision 1

1 Our PF contact force estimates exhibited similarities and differences with previously
2 published estimates. Consistent with our study, Sharma et al. (Sharma et al., 2008) reported that
3 patellar contact forces may be largely determined by TF contact forces. In contrast to our study,
4 Ward et al. (Ward and Powers, 2004) reported maximum PF contact forces on the order of 400 to
5 800 N during gait as calculated by a simpler model. Our maximum values of approximately 250
6 N were lower, possibly because our model required fewer assumptions about the interactions
7 between muscle forces and knee geometry.

8 None of the “predicted” problem formulations predicted significant lateral contact force
9 during midstance. However, sizable lateral contact forces were generated when more inverse
10 dynamic loads than just the flexion-extension torque were used as constraints. The lack of
11 significant lateral contact force during midstance may be due in part to omission of the lateral
12 collateral (LCL) and popliteofibular (PFL) ligaments in our model (Shelburne et al., 2006).
13 Morrison suggested that the LCL generates the most force during midstance (Morrison, 1970).
14 To match *in vivo* lateral contact force measurements, Kim et al. increased the pre-strain in the
15 LCL and PFL until they contributed approximately 400 N of lateral contact force during
16 midstance (Kim et al., 2009). However, intraoperative measurement of medial and lateral tibial
17 contact force during passive knee flexion suggests that collateral ligaments contribute only about
18 50 N of contact force to each side (D'Lima et al., 2007). Other possible explanations for the
19 “missing” lateral contact force are weak TFL and BFSH muscles, omission of certain muscles
20 from our model (e.g., sartorius and gracilis), omission of neighboring joints in the model (see
21 below), predicted lateral muscle activations that may be inconsistent with the subject’s actual
22 activations (Winby et al. 2009), and uncertainty over the form of the optimization cost function.

23 The reliability of muscle and contact force estimates at the knee would likely be improved
24 using a combination of optimization and EMG-driven methods (Lloyd and Besier, 2003;

Revision 1

1 Buchanan et al., 2005; Besier et al., 2009; Winby et al. 2009). Additional experimental data
2 provided by EMG measurements would make the “predicted” optimization solutions more
3 unique. While knowing the “correct” optimization cost function would become less critical, a
4 cost function would still be required to predict forces in muscles for which no EMG
5 measurements are available. Since EMG data were not available for the present study, a new
6 experimental data set is needed to investigate this possibility.

7 Estimation of muscle forces via optimization implicitly assumes that neural control of
8 movement is optimal in some sense. This assumption may be more justifiable for healthy
9 subjects than for subjects with a pathology that involves the neural control system (e.g., stroke or
10 cerebral palsy). Following total knee replacement, some patients exhibit reduced quadriceps
11 strength and activation (Mizner and Snyder-Mackler, 2005; Meier et al., 2008), and these deficits
12 lead to functional limitations. The subject who participated in our study does not have any
13 functional limitations due to quadriceps strength or activation deficits, and his gait pattern
14 appears visually normal. Quantitatively, his ground reaction force curves are similar to data
15 reported in the literature for normal subjects with healthy knees (Chao et al., 1983), and his
16 self-selected walking speed (1.24 ± 0.03 m/s) is in the range observed for normal subjects
17 (Andriacchi et al., 1982). Thus, the optimality assumption may still be reasonable for this
18 particular subject.

19 Though availability of *in vivo* contact force data provided a unique opportunity for evaluating
20 knee muscle and contact force estimates, this study still possesses a number of limitations. First,
21 only a single gait trial from a single subject was analyzed. Data from additional trials and
22 subjects are needed to assess the extent to which these results can be generalized. Second, the
23 patient used in this study had an implanted knee, so it is not known how well these results apply
24 to subjects with natural knees. We anticipate, however, that the principles elucidated by this

Revision 1

1 study will be applicable to natural knees as well. Third, ligaments (apart from the patellar
2 ligament) and contact friction were not included in the model, which may be important for
3 reducing residual loads in anterior-posterior tibial force. Fourth, alignment of the implant
4 components and bone models to their segmented points was imperfect. Fifth, bone models and
5 associated muscle and ligament origin and insertion points were taken from a different subject of
6 similar stature. Sixth, EMG measurements were not available to perform a qualitative evaluation
7 of the estimated muscle activation patterns. While these limitations may affect the ultimate goal
8 of estimating *in vivo* muscle and contact forces accurately, they do not prevent investigation of
9 how optimization problem formulation influences calculated muscle and contact forces.
10 Furthermore, reasonable agreement with the *in vivo* contact force measurements suggests that
11 our knee model was a reasonable initial representation of the subject being studied.

12 The most significant limitation in the present study is omission of neighboring joints from the
13 model. Seven of the eleven muscles in our model are biarticular, crossing the knee as well as the
14 ankle or hip. However, force-producing constraints imposed on biarticular muscles by
15 neighboring joints were not included in our problem formulations, likely affecting the calculated
16 muscle forces (Frayssé et al., 2009). For example, use of TFL to balance the frontal plane
17 moment at the hip and keep the pelvis level could contribute to increased TFL muscle force and
18 hence increased lateral contact force. Furthermore, some differences in muscle force estimates
19 from the two cost functions can be explained by indeterminacy between uniarticular and
20 biarticular muscles having similar function at the knee (e.g., VAS and RF or BFLH and BFLH).
21 Musculoskeletal modeling software capable of accommodating muscle wrapping surfaces (which
22 Autolev cannot do easily) and user-written contact routines will be needed to extend the current
23 model to include the ankle and hip. In conclusion, this study presented a novel approach for
24 predicting muscle and contact forces simultaneously in the knee during gait. The approach was

Revision 1

1 made possible by recently developed surrogate contact modeling methods. The “matched” and
2 “predicted” optimization problems demonstrated the abilities and limitations of the current
3 musculoskeletal model based on the magnitudes of the residual loads and the errors in predicted
4 TF contact forces. Demonstrating the feasibility of the simultaneous approach is an important
5 step toward the development of new methods that utilize all available experimental data in the
6 muscle and contact force estimation process for the knee.

7

8 **Conflict of Interest**

9 There are no conflicts of interest.

10

11 **Acknowledgments**

12 This work was supported by NSF CAREER award CBET 0239042 and NSF award CBET
13 0602996 to B.J. Fregly and by Australian Research Council Discovery Project grant DP0878705
14 to M.G. Pandy. The authors would like to thank J.W. Fernandez for providing the muscle origin,
15 insertion, and strength data used in this study.

16

17 **References**

18 Anderson, F.C., Pandy, M.G., 2001. Static and dynamic optimization solutions for gait are
19 practically equivalent. *Journal of Biomechanics* 34, 153-161.

20 Anderson, F.C., Pandy, M.G., 2003. Individual muscle contributions to support in normal
21 walking. *Gait and Posture* 17, 159-169.

22 Andriacchi T.P, Galante J.O., Fermier RW. 1982. The influence of total knee-replacement design
23 on walking and stair-climbing. *Journal of Bone and Joint Surgery* 64, 1328–1335

24 Banks, S.A., Fregly, B.J., Boniforti, F., Reinschmidt, C., Romagnoli, S., 2005. Comparing in

Revision 1

- 1 vivo kinematics of unicondylar and bi-unicondylar knee replacements. *Knee Surgery, Sports*
2 *Traumatology, Arthroscopy* 13, 551-556.
- 3 Bei, Y., Fregly, B.J., 2004. Multibody dynamic simulation of knee contact mechanics. *Medical*
4 *Engineering & Physics* 26, 777-789.
- 5 Besier, T.F., Fredericson, M., Gold, G.E., Beaupre, G.S., Delp, S.L., 2009. Knee muscle forces
6 during walking and running in patellofemoral pain patients and pain-free controls. *Journal of*
7 *Biomechanics* 42, 898-905.
- 8 Buchanan, T.S., Lloyd, D.G., Manal, K., Besier, T.F., 2005. Estimation of muscle forces and joint
9 moments using a forward-inverse dynamics model. *Medicine and Science in Sports Exercise*
10 37, 1911-1916.
- 11 Chao, E.Y., Laughman, R.K., Schneider, E., Stauffer R.N., 1983. Normative data of knee joint
12 motion and ground reaction forces in adult level walking. *Journal of Biomechanics* 16,
13 219-233
- 14 Crowninshield, R.D., 1978. Use of optimization techniques to predict muscle forces. *Journal of*
15 *Biomechanical Engineering* 100, 88-92.
- 16 D'Lima, D.D., Patil, S., Steklov, N., Colwell, C.W., Jr., 2007. An ABJS Best Paper: Dynamic
17 intraoperative ligament balancing for total knee arthroplasty. *Clinical Orthopaedics and*
18 *Related Research* 63, 208-212.
- 19 D'Lima, D.D., Patil, S., Steklov, N., Slamin, J.E., Colwell, C.W., Jr., 2006. Tibial forces
20 measured in vivo after total knee arthroplasty. *J Arthroplasty* 21, 255-262.
- 21 D'Lima, D.D., Patil, S., Steklov, N., Slamin, J.E., Colwell, C.W.J., 2005a. The Chitranjan
22 Ranawat Award: In vivo knee forces after total knee arthroplasty. *Clinical Orthopaedics and*
23 *Related Research* 440, 45-49.
- 24 D'Lima, D.D., Townsend, C.P., Arms, S.W., Morris, B.A., Colwell, C.W.J., 2005b. An

Revision 1

- 1 implantable telemetry device to measure intra-articular tibial forces. *Journal of Biomechanics*
2 38, 299-304.
- 3 Fraysse, F., Dumas, R., Cheze, L., Wang, X., 2009. Comparison of global and joint-to-joint
4 methods for estimating the hip joint load and the muscle forces during walking. *Journal of*
5 *Biomechanics* (in press).
- 6 Glitsch, U., Baumann, W., 1997. The three-dimensional determination of internal loads in the
7 lower extremity. *Journal of Biomechanics* 30, 1123-1131.
- 8 Herzog, W., Longino, D., Clark, A., 2003. The role of muscles in joint adaptation and
9 degeneration. *Langenbeck's Archives Surgery* 388, 305-315.
- 10 Jinha, A., Ait-Haddou, R., Herzog, W., 2006. Predictions of co-contraction depend critically on
11 degrees-of-freedom in the musculoskeletal model. *Journal of Biomechanics* 39, 1145-1152.
- 12 Kaufman, K.R., An, K.W., Litchy, W.J., Chao, E.Y., 1991. Physiological prediction of muscle
13 forces--I. Theoretical formulation. *Neuroscience Letters* 40, 781-792.
- 14 Kaufman, K.R., Kovacevic, N., Irby, S.E., Colwell, C.W., 1996. Instrumented implant for
15 measuring tibiofemoral forces. *J Biomech* 29, 667-671.
- 16 Kim, H.J., Fernandez, J.W., Akbarshahi, M., Walter, J.P., Fregly, B.J., M.G., P., 2009. Evaluation
17 of predicted knee-joint muscle forces during gait using an instrumented knee implant. *Journal*
18 *of Orthopaedic Research* 27, 1326-1331.
- 19 Lin, Y.-C., Farr, J., Carter, K., Fregly, B.J., 2006. Response surface optimization for joint contact
20 model evaluation. *Journal of Applied Biomechanics* 22, 120-130.
- 21 Lin, Y.-C., Haftka, R.T., Queipo, N.V., Fregly, B.J., 2008. Dynamic simulation of knee motion
22 using three-dimensional surrogate contact modeling. In, *Proceedings of the 2008 Summer*
23 *Bioengineering Conference*. San Marco Island, Florida: The American Society of Mechanical
24 Engineers, SBC2008-190966.

Revision 1

- 1 Lin, Y.-C., Haftka, R.T., Queipo, N.V., Fregly, B.J., 2009. Two-dimensional surrogate contact
2 modeling for computationally efficient dynamic simulation of total knee replacements.
3 *Journal of Biomechanical Engineering* 131, 041010-041011 - 041010-041018.
- 4 Liu, M.Q., Anderson, F.C., Schwartz, M.H., Delp, S.L., 2008. Muscle contributions to support
5 and progression over a range of walking speeds. *Journal of Biomechanics* 41, 3243-3252.
- 6 Lloyd, D.G., Besier, T.F., 2003. An EMG-driven musculoskeletal model to estimate muscle
7 forces and knee joint moments in vivo. *Journal of Biomechanics* 36, 765-776.
- 8 Meier, W., Mizner, R.L., Marcus, R.L., Dibble, L.E., Peters, C., and Lastayo, P.C., 2008. Total
9 knee arthroplasty: muscle impairments, functional limitations, and recommended
10 rehabilitation approaches. *Journal of Orthopaedic and Sports Physical Therapy* 38, 246-256.
- 11 Mizner, R.L. and Snyder-Mackler, L., 2005. Altered loading during walking and sit-to-stand is
12 affected by quadriceps weakness after total knee arthroplasty *Journal of Orthopaedic*
13 *Research* 23, 1083-1090.
- 14 Morrison, J.B., 1970. The mechanics of the knee joint in relation to normal walking. *Journal of*
15 *Biomechanics* 3, 51-61.
- 16 Neptune, R.R., Zajac, F.E., Kautz, S.A., 2004. Muscle force redistributes segmental power for
17 body progression during walking. *Gait and Posture* 19, 194-205.
- 18 Praemer, A., Furner, S., Rice, D.P., 1999. *Musculoskeletal Conditions in the United States.*
19 *American Academy of Orthopaedic Surgeons, Rosemont, IL.*
- 20 Reeves, N.D., Narici, M.V., Maganaris, C.N., 2003. Strength training alters the viscoelastic
21 properties of tendons in elderly humans. *Muscle Nerve* 28, 74-81.
- 22 Reinbolt, J.A., Haftka, R.T., Chmielewski, T.L., Fregly, B.J., 2008. A computational framework
23 to predict post-treatment outcome for gait-related disorders. *Medical Engineering & Physics*
24 30, 434-443.

Revision 1

- 1 Reinbolt, J.A., Schutte, J.F., Fregly, B.J., Koh, B.-I., Haftka, R.T., George, A.D., Mitchell, K.H.,
2 2005. Determination of patient-specific multi-joint kinematic models through two-level
3 optimization. *Journal of Biomechanics* 38, 621-626.
- 4 Schultz, A.B., Andersson, G.B.J., 1981. Analysis of loads on the lumbar spine. *Spine* 6, 76-82.
- 5 Sharma, A., Leszko, F., Komistek, R.D., Scuderi, G.R., Cates, H.E.J., Liu, F., 2008. In vivo
6 patellofemoral forces in high flexion total knee arthroplasty. *Journal of Biomechanics* 41,
7 642-648.
- 8 Shelburne, K.B., Pandy, M.G., Anderson, F.C., Torry, M.R., 2004. Pattern of anterior cruciate
9 ligament force in normal walking. *Journal of Biomechanics* 37, 797-805.
- 10 Shelburne, K.B., Torry, M.R., Pandy, M.G., 2005. Muscle, ligament, and joint-contact forces at
11 the knee during walking. *Medicine and Science in Sports and Exercise* 37, 1948-1956.
- 12 Shelburne, K.B., Torry, M.R., Pandy, M.G., 2006. Contributions of muscles, ligaments, and the
13 ground-reaction force to tibiofemoral joint loading during normal gait. *Journal of*
14 *Orthopaedic Research* 24, 1983-1990.
- 15 Taylor, W., Heller, M., Bergmann, G., Duda, G., 2004. Tibio-femoral loading during human gait
16 and stair climbing. *Journal of Orthopaedic Research* 22, 625-632.
- 17 Ward, S.R., Powers, C.M., 2004. The influence of patella alta on patellofemoral joint stress
18 during normal and fast walking. *Clinical Biomechanics* 19, 1040-1047.
- 19 Winby, C.R., Lloyd, D.G., Besier, T.F., and Kirk, T.B. (2009) Muscle and external load
20 contribution to knee joint contact loads during normal gait. *Journal of Biomechanics* 42,
21 2294–2300.
- 22 Zhao, D., Banks, S.A., D'Lima, D.D., Colwell Jr., C.W., Fregly, B.J., 2007a. In vivo medial and
23 lateral tibial loads during dynamic and high flexion activities. *Journal of Orthopaedic*
24 *Research* 25, 593-602.

Revision 1

- 1 Zhao, D., Banks, S.A., Mitchell, K.H., D'Lima, D.D., Colwell, C.W., Fregly, B.J., 2007b.
- 2 Correlation between the knee adduction torque and medial contact force for a variety of gait
- 3 patterns. *Journal of Orthopaedic Research* 25, 789-797.

4

5

1 **Figure Captions**

2

3 Figure 1: Twelve degree-of-freedom knee model combining muscle, articular contact, and
4 dynamic skeletal models. The model is controlled by 11 muscles and incorporates tibiofemoral
5 and patellofemoral contact. Compressive contact force on the tibia (patella) is defined as the
6 component of net contact force acting perpendicular to the planar back surface of the
7 polyethylene tibial insert (patellar button).

8

9 Figure 2: Visual depiction of the steps involved in creating the patient-specific implant/bone
10 geometric model. a) Segmentation of implant components and bones from post-surgery CT data.
11 b) Alignment of MR-derived bone models from a different subject with the segmented bones. c)
12 Alignment of metallic implant CAD models to the segmented implant components. d)
13 Positioning of polyethylene implant components on tibial baseplate and patella and deletion of
14 segmented points. All geometry registration was performed using Geomagic Studio (Raindrop
15 Geomagic, Research Triangle Park, NC).

16

17 Figure 3: Animation sequence (left to right) of the static analysis used to register the
18 patient-specific full-leg inverse dynamic model to the patient-specific implant-bone geometric
19 model. Five stiff springs (dotted lines) between corresponding anatomic points were used to pull
20 the inverse dynamic model onto the geometric model.

21

22 Figure 4: Comparison of measured (gray bands) and estimated (solid and dotted lines) *in vivo*
23 compressive contact forces for the eight “matched” optimization problems. Each column
24 represents a different constraint set defined in Table 1. Estimates overlay *in vivo* measurements

Revision 1

1 for medial, lateral, and total compressive contact force. No *in vivo* patellar compressive contact
 2 force measurements were available.

3

4 Figure 5: Estimated muscle forces for the eight “matched” optimization problems. Each column
 5 represents a different constraint set defined in Table 1.

6

7 Figure 6: Comparison of measured (gray bands) and estimated (solid and dotted lines) *in vivo*
 8 compressive contact forces for the eight “predicted” optimization problems. Each column
 9 represents a different constraint set defined in Table 1. No *in vivo* patellar compressive contact
 10 force measurements were available.

11

12 Figure 7: Estimated muscle forces for the eight “predicted” optimization problems. Each column
 13 represents a different constraint set defined in Table 1.

14

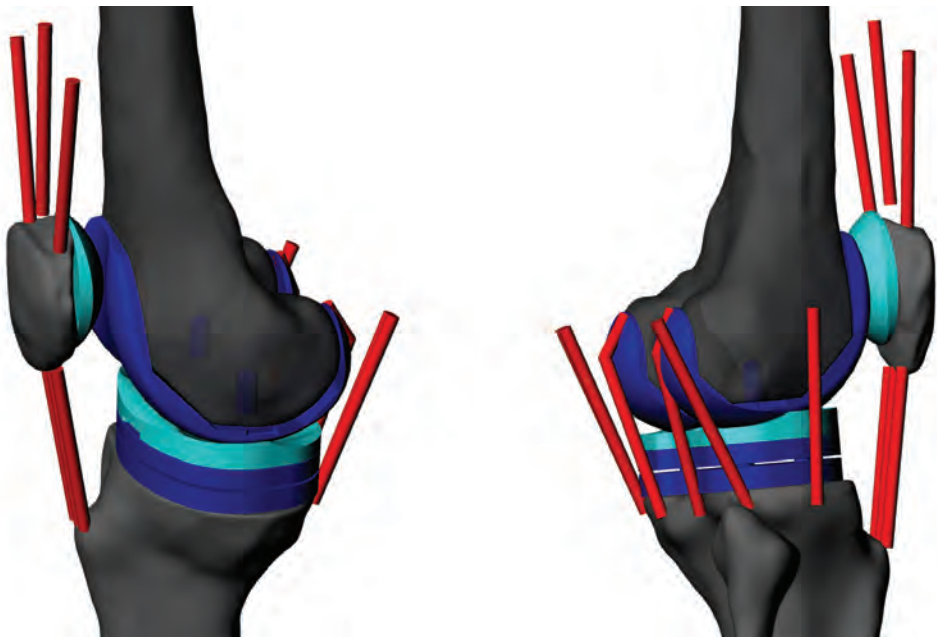
15 **Table Captions**

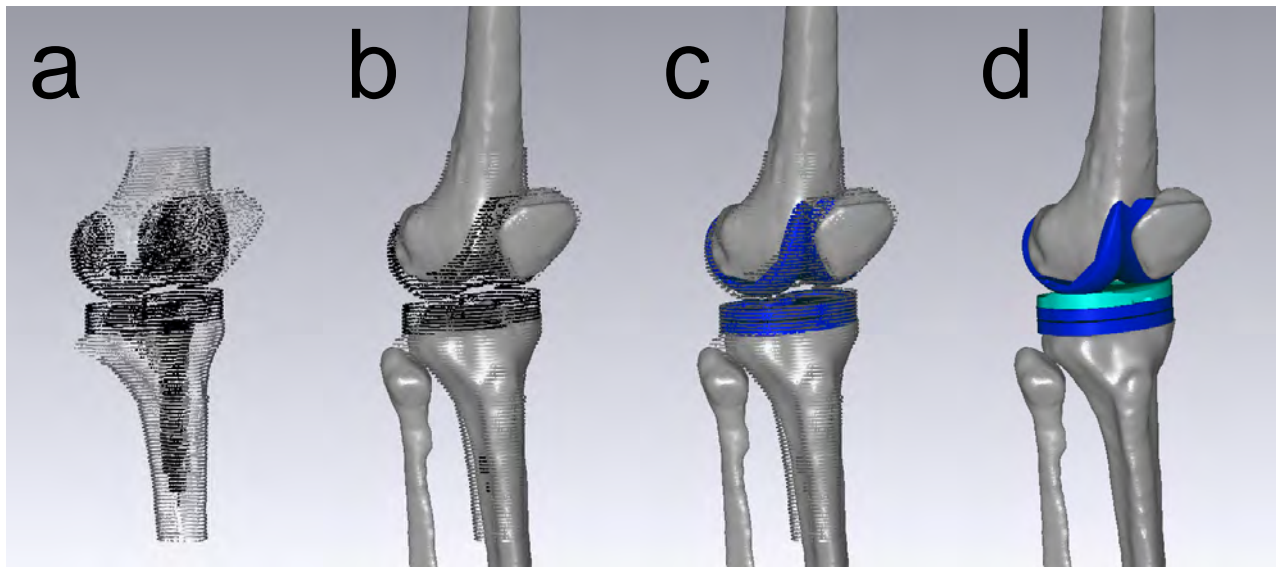
16

17 Table 1: Summary of the four optimization constraints sets composed of different combinations
 18 of three tibial residual loads. Residual loads are for the flexion-extension torque ($T_{Tibia\ FE}^{Residual}$), the
 19 anterior-posterior force ($F_{Tibia\ AP}^{Residual}$), and the internal-external torque ($T_{Tibia\ IE}^{Residual}$). The residual
 20 flexion-extension torque was included in all four constraint sets since it is the most commonly
 21 used constraint for predicting muscle forces at the knee.

22

23 Table 2: Root-mean-square difference in solutions generated by the two cost functions as more
 24 inverse dynamic loads were added as constraints.





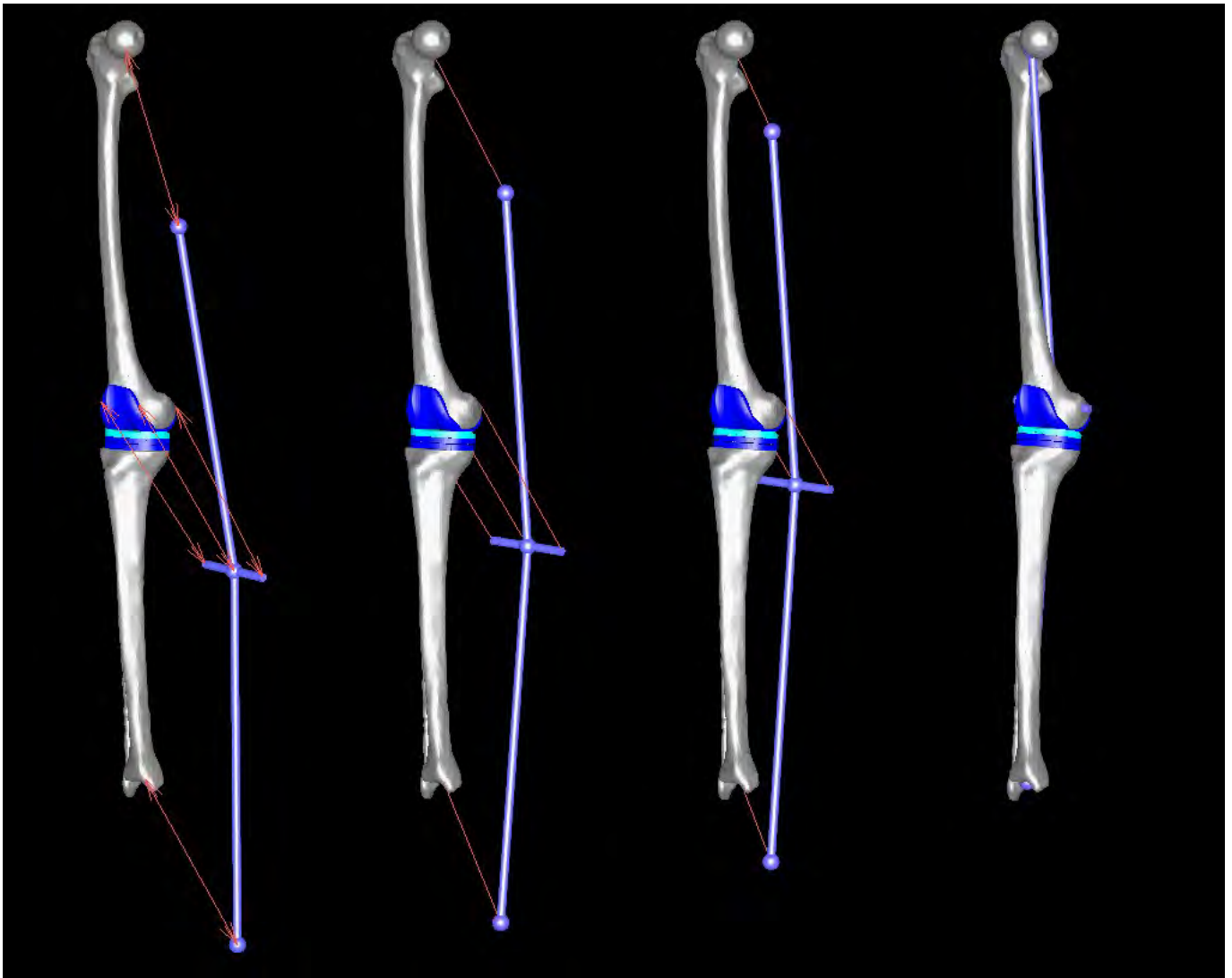


Figure 4

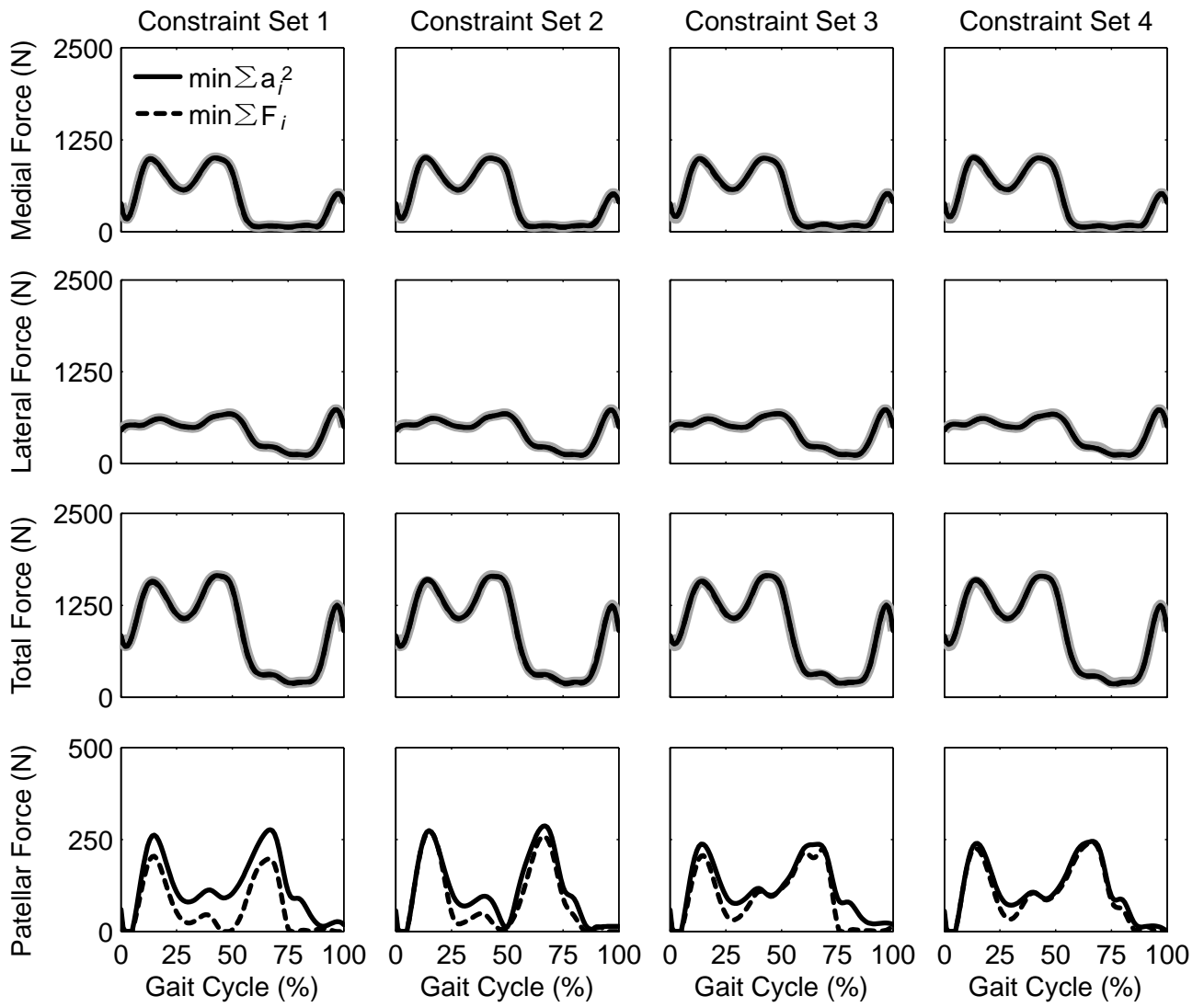


Figure 5

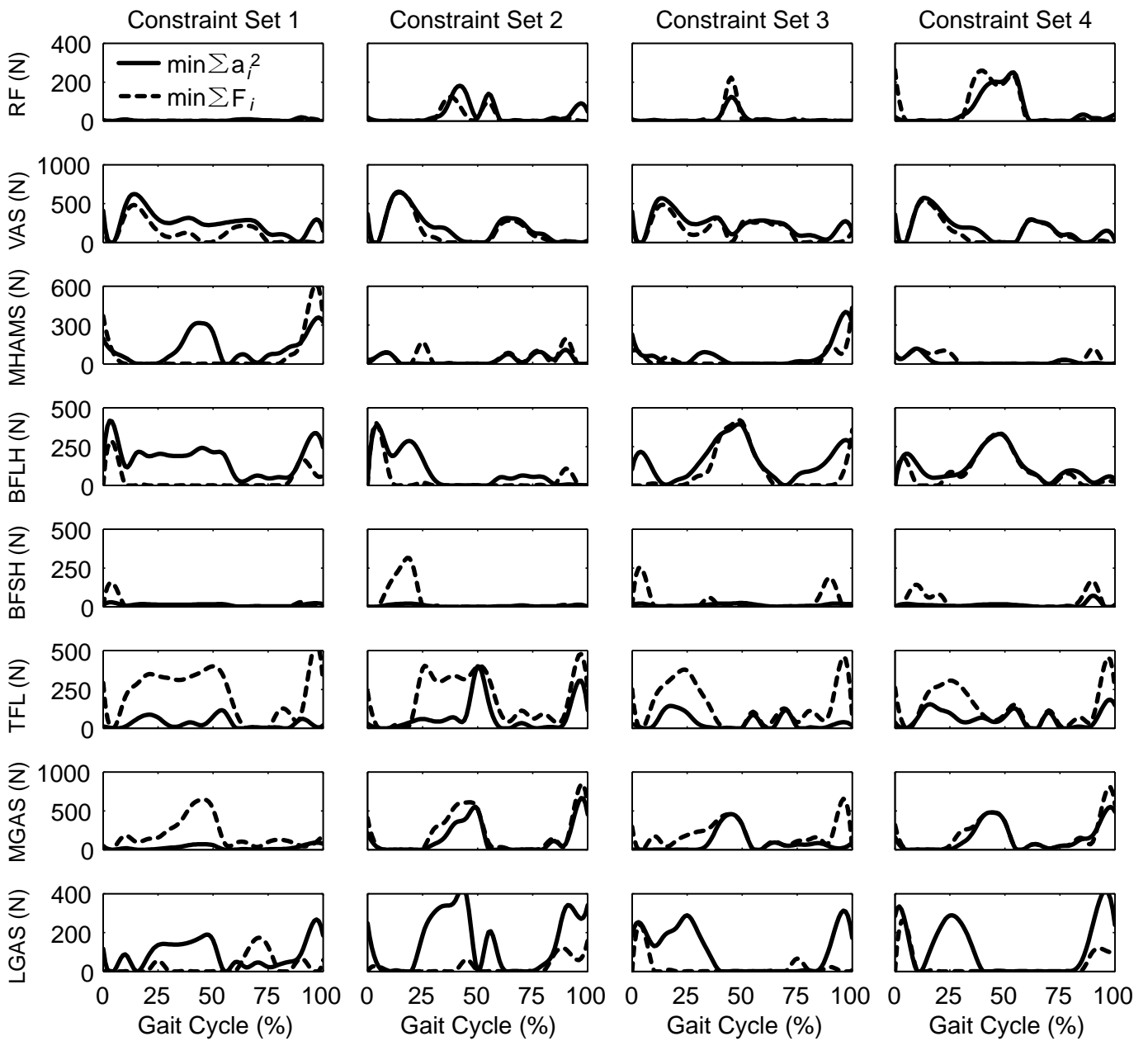


Figure 6

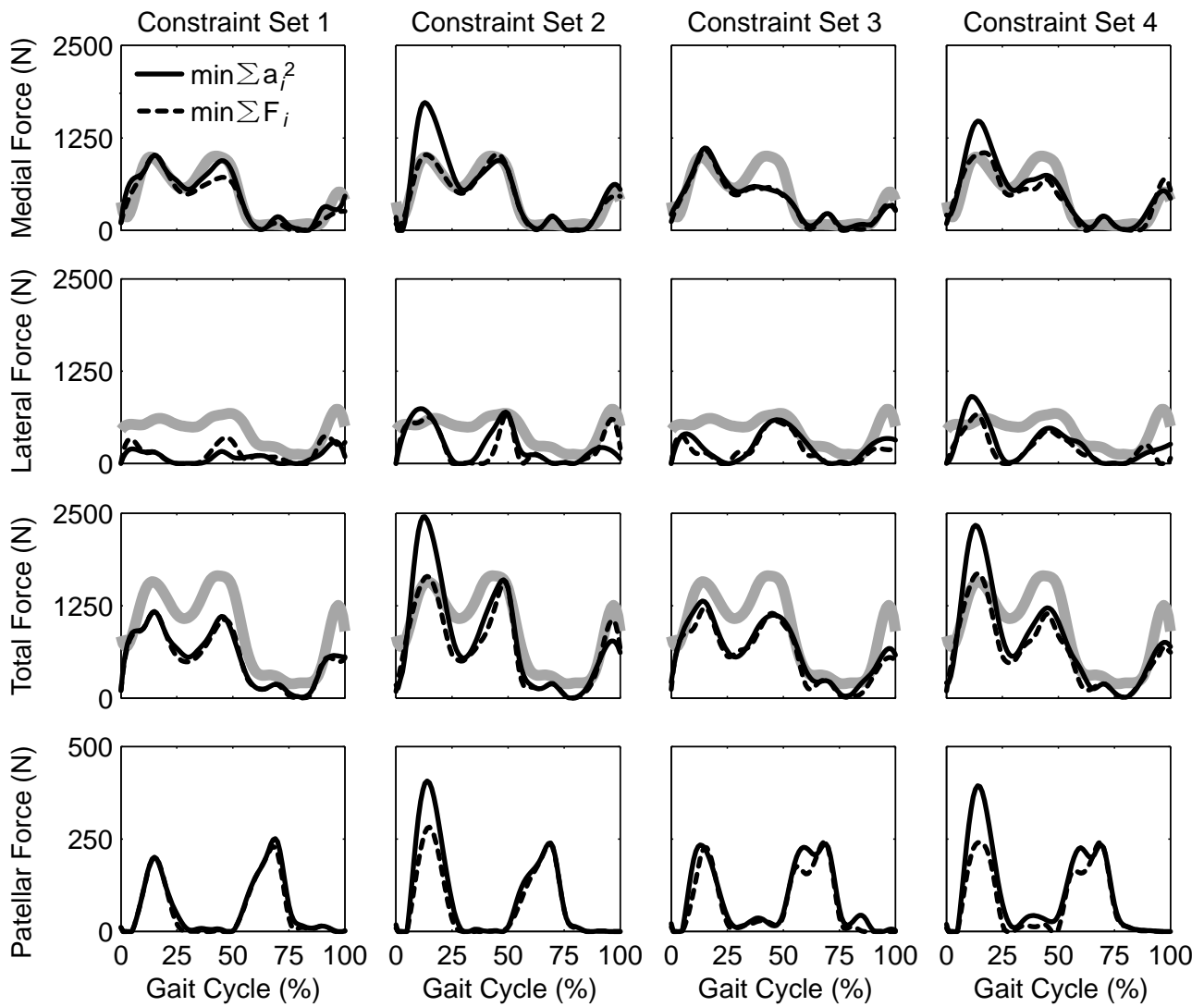
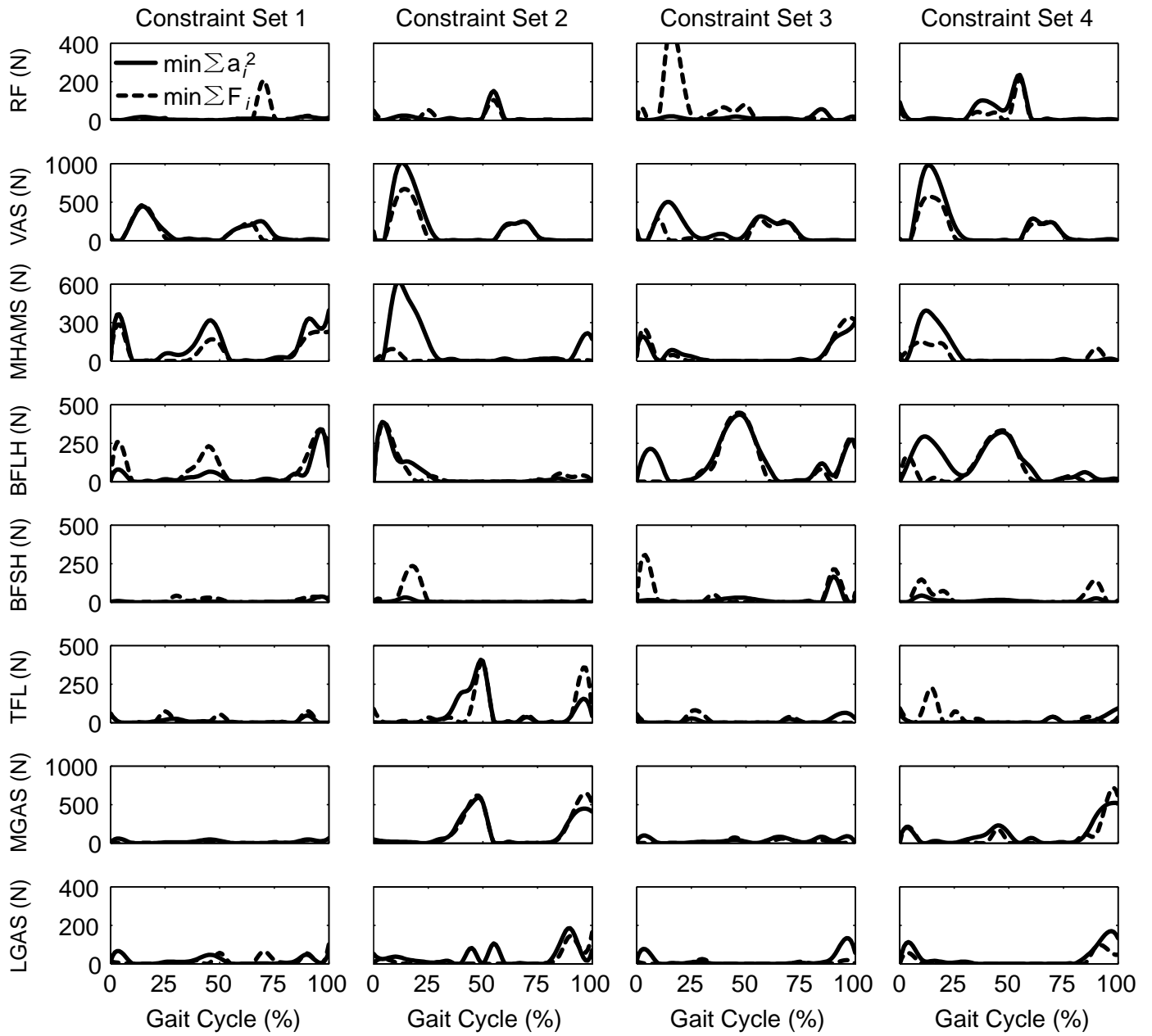


Figure 7



Constraint Set	$T_{Tibia\ FE}^{Residual}$	$F_{Tibia\ AP}^{Residual}$	$T_{Tibia\ IE}^{Residual}$
1	✓		
2	✓	✓	
3	✓		✓
4	✓	✓	✓

“Matched” Solutions

Constraint Set	Muscle Forces	Medial Contact Force	Lateral Contact Force	Total Contact Force	Patellar Contact Force
1	152.28	7.39	3.70	9.55	64.74
2	109.28	8.87	3.11	11.23	32.69
3	112.85	7.48	3.08	9.70	34.78
4	84.88	7.37	3.48	8.33	16.56

“Predicted” Solutions

Constraint Set	Muscle Forces	Medial Contact Force	Lateral Contact Force	Total Contact Force	Patellar Contact Force
1	44.67	104.34	92.98	44.52	12.17
2	86.91	231.24	134.41	277.76	42.63
3	74.74	40.47	77.02	93.68	27.31
4	72.83	146.71	122.22	233.25	48.80

SUPPLEMENTARY MATERIAL

In this section, we provide additional details on construction of the musculoskeletal knee model and formulation of the static optimization problems. These details are intended for the interested reader who wishes to understand more thoroughly our method for simultaneous prediction of muscle and contact forces in the knee.

Additional Details on Musculoskeletal Model Development

The key technical element that made the present study possible was the use of surrogate contact models for the tibiofemoral and patellofemoral joints. Construction of surrogate models for elastic contact problems poses unique challenges, which are addressed in our recent publications in this area (Lin et al., 2008; Lin et al., 2009). Conceptually, a surrogate contact model is a computationally cheap contact model that matches input-output relationships sampled from a computationally expensive contact model. For the present study, surrogate contact models were constructed to reproduce load-displacement relationships sampled from elastic foundation (EF) contact models of the subject's implant components using linear elastic material properties (Bei and Fregly, 2004). For the TF joint, separate surrogate contact models were created for the medial and lateral compartment, while for the PF joint, a single surrogate contact model was created. Each surrogate contact model took six pose parameters (i.e., three translations and three rotations) as inputs, where the pose parameters defined the relative position and orientation of the tibial insert or patellar button with respect to the femoral component, and output six corresponding contact loads (i.e., three forces and three torques). Sample points inputs to the elastic foundation contact models non-uniformly distributed over a six-dimensional design space were generated using a Hammersley quasirandom sequence (Hammersley, 1960), while fitting of the resulting input-output relationships was performed using the DACE Kriging Toolbox

(Lophaven et al., 2002). For all surrogate contact models, y translation corresponded to the approximate contact normal direction for the polyethylene, z translation to a medial-lateral direction, and x translation was defined as $y \times z$ (Fig. S1).

The process used to register the patient-specific inverse dynamic skeletal model to the patient-specific geometric implant/bone model (Fig. 2) also warrants a more detailed description. Creation of the patient-specific implant/bone model was performed as a four-step process. First, the patient's bones (tibia, fibula, femur, and patella) and metallic implant components (tibial tray, femoral component) were segmented from the patient's post-surgery CT data. Second, MR-derived bone surface models (including muscle and ligament origins and insertions) from a different subject of comparable stature were aligned to the patient's segmented bones. Third, CAD models of the metallic implant components were aligned to the patient's segmented implant components. Fourth, CAD models of the polyethylene tibial insert and patellar button were aligned to the tibial tray and drill holes on the posterior surface of the patella, respectively. In the resulting model, ankle and hip centers were estimated from bone geometry, while a best-fit knee center and functional flexion-extension axis were calculated from the fluoroscopic motion data for treadmill gait.

Creation of the patient-specific skeletal model was performed using established optimization methods (Reinbolt et al., 2005; Reinbolt et al., 2008). The skeletal model was a dynamic, 27 degree-of-freedom (DOF) full-body walking model (Fregly et al., 2007) (Fig. S2). Segment coordinate systems within the body segments (lower extremities, pelvis, trunk, and upper extremities) were created using marker data from a static trial. Joint positions and orientations in adjacent body segments were then determined for the ankle (two non-intersecting pin joints), knee (pin joint), and hip (ball-and-socket joint) on each side (right and left) using marker data from isolated joint motion trials. Finally, segment mass properties (masses, mass centers, and

moments of inertia) and lower extremity joint positions and orientations were adjusted simultaneously using marker and ground reaction data from the selected overground gait trial. The resulting full-body model with joint constraints minimized errors between model and experimental marker locations over all time frames while simultaneously minimizing residual loads acting on the pelvis segment.

Once both models were constructed, the right thigh and shank of the inverse dynamic model were registered to the femur and tibia/fibula of the geometric model by performing a static analysis (Fig. 3). Five stiff springs were connected between corresponding points (ankle, knee, and hip center and medial and lateral side of the best-fit knee flexion-extension axis) on the two models, the static analysis pulled the inverse dynamic model onto the geometric model by minimizing the potential energy in the springs. During the registration process, the internal configuration of the inverse dynamic model was locked to match the subject's standing static pose while the knee in the geometric model was flexed relative to the grounded femur. After registration, the implant and bone geometry were transferred to the inverse dynamic model, the knee functional flexion-extension axis was unconstrained to allow 6 DOFs, and the patella was added to the model in a position consistent with the post-surgery CT scan data to provide the remaining 6 DOFs.

Additional Details on Muscle and Contact Force Estimation

While the two-level optimization approach used to estimate muscle and contact force simultaneously was described in general terms in the manuscript, a more explicit description including the relevant equations may be helpful for individuals interested implementing this approach.

The cost function for the inner-level optimization minimized the sum of squares of selected

residual loads acting on the tibia and patella. Each net force and torque acting on these bones was assumed to be balanced by a combination of muscle, contact, and patellar ligament forces,

$$\begin{aligned} F_{ij}^{Net} &= F_{ij}^{Muscle} + F_{ij}^{Contact} + F_{ij}^{Ligament} \\ T_{ij}^{Net} &= T_{ij}^{Muscle} + T_{ij}^{Contact} + T_{ij}^{Ligament} \end{aligned} \quad (1)$$

where subscript i represents a particular bone (tibia or patella) and subscript j a particular direction (x , y , or z) within that bone. For the tibia, net forces and torques were calculated from the inverse dynamic skeletal model, while for the patella, these quantities were assumed to be zero. Residual loads were defined as differences between the known net loads and the loads produced by the current muscle, contact, and patellar ligament forces:

$$\begin{aligned} F_{ij}^{Residual} &= F_{ij}^{Net} - (F_{ij}^{Muscle} + F_{ij}^{Contact} + F_{ij}^{Ligament}) \\ T_{ij}^{Residual} &= T_{ij}^{Net} - (T_{ij}^{Muscle} + T_{ij}^{Contact} + T_{ij}^{Ligament}) \end{aligned} \quad (2)$$

To find the static configuration for the current muscle activations a , the inner-level cost function minimized three of the six residual loads acting on the tibia and all six residual loads acting on the patella by making small adjustments to the nine corresponding pose parameters q (Fig. S3):

$$\begin{aligned} \min_q \left\{ \left(w_F F_{Tibia\ y}^{Residual}(q, a) \right)^2 + \left(w_F F_{Tibia\ z}^{Residual}(q, a) \right)^2 + \left(w_T T_{Tibia\ x}^{Residual}(q, a) \right)^2 \right. \\ \left. + \sum_j \left[\left(w_F F_{Patella\ j}^{Residual}(q, a) \right)^2 + \left(w_T T_{Patella\ j}^{Residual}(q, a) \right)^2 \right] \right\} \end{aligned} \quad (3)$$

In this equation, w_F and w_T are weight factors used to normalize force by body weight and torque by percent body weight times height. Three residual loads acting on the tibia were omitted because tibial contact forces have been shown to be insensitive to small changes in the corresponding pose parameters (i.e., x translation, y rotation, and z rotation) (Fregly et al., 2008).

The outer-level optimization used two cost functions and four constraint sets to investigate how optimization problem formulation affects the estimated muscle and contact forces (Glitsch and Baumann, 1997; Jinha et al., 2006). The equations for these cost functions and constraint

sets are provided below, where F_{Medial}^{Comp} is medial tibiofemoral compressive contact force, $F_{Lateral}^{Comp}$ is lateral tibiofemoral compressive contact force, and $F_{Patella}^{Comp}$ is patellar compressive contact force, and a represents the eight muscle activation design variables (Fig. S3):

$$\begin{aligned}
\text{Cost function 1: } & \min_a \left\{ \sum_{i=1}^8 a_i^2 + \text{selected constraint set} \right\} \\
\text{Cost function 2: } & \min_a \left\{ w_F |F_{Medial}^{Comp}(a)| + w_F |F_{Lateral}^{Comp}(a)| + w_F |F_{Patella}^{Comp}(a)| + \text{selected constraint set} \right\} \\
\text{Constraint set 1: } & \left(w_T T_{Tibia\ z}^{Residual}(a) \right)^2 \\
\text{Constraint set 2: } & \left(w_T T_{Tibia\ z}^{Residual}(a) \right)^2 + \left(w_F F_{Tibia\ x}^{Residual}(a) \right)^2 \\
\text{Constraint set 3: } & \left(w_T T_{Tibia\ z}^{Residual}(a) \right)^2 + \left(w_T T_{Tibia\ y}^{Residual}(a) \right)^2 \\
\text{Constraint set 4: } & \left(w_T T_{Tibia\ z}^{Residual}(a) \right)^2 + \left(w_F F_{Tibia\ x}^{Residual}(a) \right)^2 + \left(w_T T_{Tibia\ y}^{Residual}(a) \right)^2
\end{aligned} \tag{4}$$

The residual flexion-extension torque $T_{Tibia\ z}^{Residual}$ was included in all four constraint sets since it is the most commonly used constraint for predicting muscle forces at the knee. Due to the lack of contact force sensitivity, the three pose parameters corresponding to the three residual loads appearing in Eq. (4) were fixed at values consistent with the best-fit flexion-extension axis. Muscle activations were bounded to be between zero and infinity (rather than the physiological upper bound of one) so that insufficient strength in one or more muscles would not prevent the outer-level optimization from finding a feasible solution.

The eight outer-level optimization problem formulations defined by Eq. (4) were solved two ways – with and without additional constraints to match the *in vivo* medial and lateral contact force measurements (Table 1):

$$\text{Additional constraints: } \left(w_F \Delta F_{Medial}^{Comp}(a) \right)^2 + \left(w_F \Delta F_{Lateral}^{Comp}(a) \right)^2 \tag{5}$$

In this equation, ΔF_{Medial}^{Comp} and $\Delta F_{Lateral}^{Comp}$ represent the difference between the measured and estimated compressive contact force on the medial and lateral side, respectively. These two formulations are the “matched” and “predicted” formulations described in the manuscript.

Tabulated results for residual loads and medial and lateral contact force errors for each of the 16 optimization problems are provided in Tables S1 and S2.

Supplementary References

- Bei, Y., Fregly, B.J., 2004. Multibody dynamic simulation of knee contact mechanics. *Medical Engineering & Physics* 26, 777-789.
- Fregly, B.J., Banks, S.A., D'Lima, D.D., Colwell, C.W., 2008. Sensitivity of knee replacement contact calculations to kinematic measurement errors. *Journal of Orthopaedic Research* 26, 1173-1179.
- Fregly, B.J., Reinbolt, J.A., Rooney, K.L., Mitchell, K.H., Chmielewski, T.L., 2007. Design of patient-specific gait modifications for knee osteoarthritis rehabilitation. *IEEE Transactions on Biomedical Engineering* 54, 1687-1695.
- Glitsch, U., Baumann, W., 1997. The three-dimensional determination of internal loads in the lower extremity. *Journal of Biomechanics* 30, 1123-1131.
- Hammersley, J., 1960. Monte Carlo methods for solving multivariable problems. *Proceedings of the New York Academy of Science* 86, 844-874.
- Jinha, A., Ait-Haddou, R., Herzog, W., 2006. Predictions of co-contraction depend critically on degrees-of-freedom in the musculoskeletal model. *Journal of Biomechanics* 39, 1145-1152.
- Lin, Y.-C., Haftka, R.T., Queipo, N.V., Fregly, B.J., 2008. Dynamic simulation of knee motion using three-dimensional surrogate contact modeling. In, *Proceedings of the 2008 Summer Bioengineering Conference*. San Marco Island, Florida: The American Society of Mechanical Engineers, pp. SBC2008-190966.

- Lin, Y.-C., Haftka, R.T., Queipo, N.V., Fregly, B.J., 2009. Two-dimensional surrogate contact modeling for computationally efficient dynamic simulation of total knee replacements. *Journal of Biomechanical Engineering* 131, 041010-041011 - 041010-041018.
- Lophaven, S.N., Nielsen, H.B., Søndergaard, J., 2002. DACE-A Matlab Kriging Toolbox. In, Technical Report IMM-TR-2002-13, Informatics and Mathematical Modelling: Technical University of Denmark.
- Reinbolt, J.A., Haftka, R.T., Chmielewski, T.L., Fregly, B.J., 2008. A computational framework to predict post-treatment outcome for gait-related disorders. *Medical Engineering & Physics* 30, 434-443.
- Reinbolt, J.A., Schutte, J.F., Fregly, B.J., Koh, B.-I., Haftka, R.T., George, A.D., Mitchell, K.H., 2005. Determination of patient-specific multi-joint kinematic models through two-level optimization. *Journal of Biomechanics* 38, 621-626.

Supplementary Figure and Table Captions

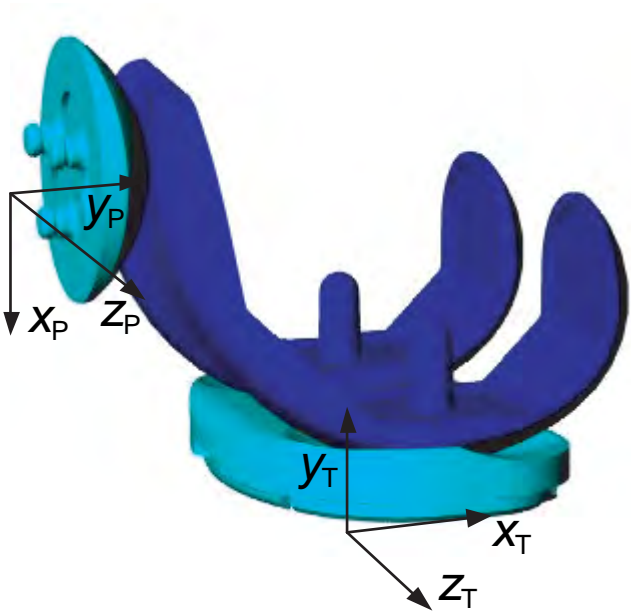
Figure S1: Segment coordinate systems used to define the direction of compressive contact force (-y) for the tibia (subscript T) and patella (subscript P). The y direction for each polyethylene component is defined to be perpendicular to the planar back surface of the component.

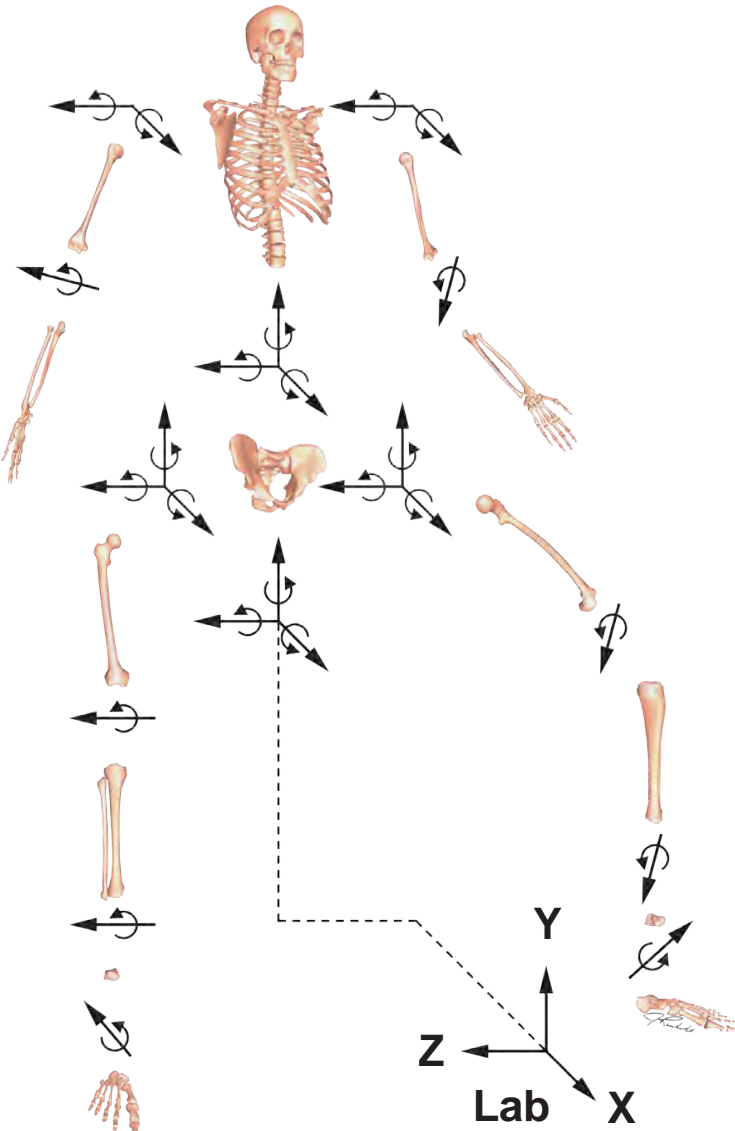
Figure S2: Dynamic patient-specific full-body walking model possessing 27 degrees of freedom (DOFs) and used for calculating inverse dynamic loads. The right leg of this model was registered to the patient-specific geometric implant/bone model to create the 12 DOF musculoskeletal knee model used for estimating muscle and contact forces.

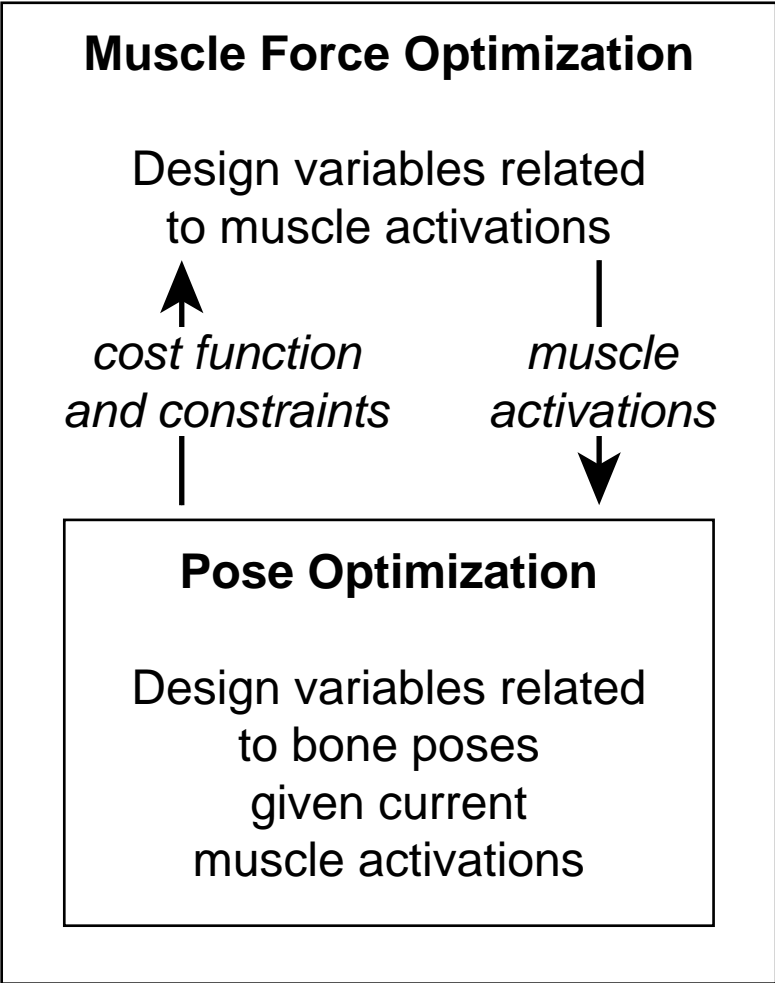
Figure S3: Overview of the two-level optimization approach used to predict muscle and contact forces simultaneously in the knee. The inner-level pose optimization determines the static configuration of the tibia and patella on the femur given the current guess for the muscle activations from the outer-level muscle optimization. The outer-level muscle optimization uses the cost function and constraints returned by the inner-level pose optimization.

Table S1: Root-mean-square residual loads from the inner-level pose optimization. Reported values are N for force and Nm for torque.

Table S2: Root-mean-square residual loads and root-mean-square errors in tibiofemoral contact forces from the outer-level muscle force optimization. Reported values are N for force and Nm for torque.







“Matched” Solutions

Constraint Set	Cost Function	$F_{Tibia\ y}^{Residual}$	$F_{Tibia\ z}^{Residual}$	$T_{Tibia\ x}^{Residual}$	$F_{Patella\ x}^{Residual}$	$F_{Patella\ y}^{Residual}$	$F_{Patella\ z}^{Residual}$	$T_{Patella\ x}^{Residual}$	$T_{Patella\ y}^{Residual}$	$T_{Patella\ z}^{Residual}$
1	$\min \sum a_i^2$	0.00	0.00	0.00	0.00	0.00	0.03	0.00	0.00	0.00
	$\min \sum F_i$	0.00	0.00	0.00	0.01	0.02	0.38	0.01	0.00	0.00
2	$\min \sum a_i^2$	0.01	0.00	0.00	0.02	0.01	0.26	0.00	0.00	0.00
	$\min \sum F_i$	0.03	0.02	0.00	0.15	0.17	0.04	0.00	0.00	0.00
3	$\min \sum a_i^2$	0.00	0.00	0.00	0.00	0.00	0.00	0.00	0.00	0.00
	$\min \sum F_i$	0.00	0.00	0.00	0.00	0.00	0.03	0.00	0.00	0.00
4	$\min \sum a_i^2$	0.00	0.00	0.00	0.96	1.94	0.22	0.00	0.01	0.02
	$\min \sum F_i$	0.00	0.00	0.00	0.45	0.68	0.06	0.00	0.00	0.01

“Predicted” Solutions

Constraint Set	Cost Function	$F_{Tibia\ y}^{Residual}$	$F_{Tibia\ z}^{Residual}$	$T_{Tibia\ x}^{Residual}$	$F_{Patella\ x}^{Residual}$	$F_{Patella\ y}^{Residual}$	$F_{Patella\ z}^{Residual}$	$T_{Patella\ x}^{Residual}$	$T_{Patella\ y}^{Residual}$	$T_{Patella\ z}^{Residual}$
1	$\min \sum a_i^2$	1.11	2.15	0.00	0.48	0.41	0.43	0.01	0.01	0.00
	$\min \sum F_i$	0.34	1.81	0.00	0.32	0.01	0.17	0.00	0.00	0.00
2	$\min \sum a_i^2$	1.57	1.92	0.03	1.31	0.56	0.17	0.00	0.02	0.01
	$\min \sum F_i$	0.38	2.42	0.00	0.32	0.12	0.14	0.00	0.00	0.00
3	$\min \sum a_i^2$	0.53	1.01	0.00	0.22	0.10	0.09	0.00	0.00	0.00
	$\min \sum F_i$	1.58	2.09	0.00	0.69	0.21	0.16	0.00	0.00	0.01
4	$\min \sum a_i^2$	0.30	0.90	0.00	0.47	0.66	0.23	0.00	0.00	0.01
	$\min \sum F_i$	0.55	1.81	0.00	0.51	0.39	0.14	0.00	0.00	0.00

“Matched” Solutions

Constraint Set	Cost Function	$T_{Tibia\ z}^{Residual}$	$F_{Tibia\ x}^{Residual}$	$T_{Tibia\ y}^{Residual}$	F_{Medial}^{Comp}	$F_{Lateral}^{Comp}$
1	$\min \sum a_i^2$	0.09	138.13	2.98	7.23	6.09
	$\min \sum F_i$	0.1	117.49	2.91	8.21	8.13
2	$\min \sum a_i^2$	0.23	83.91	3.31	10.55	7.96
	$\min \sum F_i$	0.22	82.11	3.03	12.81	8.79
3	$\min \sum a_i^2$	0.14	138.69	0.32	15.69	8.79
	$\min \sum F_i$	0.16	136.9	0.33	14.36	9.26
4	$\min \sum a_i^2$	0.27	115.52	0.63	15.21	11.02
	$\min \sum F_i$	0.27	113.38	0.67	13.46	11.75

“Predicted” Solutions

Constraint Set	Cost Function	$T_{Tibia\ z}^{Residual}$	$F_{Tibia\ x}^{Residual}$	$T_{Tibia\ y}^{Residual}$	F_{Medial}^{Comp}	$F_{Lateral}^{Comp}$
1	$\min \sum a_i^2$	0.02	115.87	3.38	136.97	398.78
	$\min \sum F_i$	0.07	122.35	2.12	154.83	356.05
2	$\min \sum a_i^2$	0.19	70.91	2.94	253.24	292.93
	$\min \sum F_i$	0.21	77.91	2.66	92.82	313.1
3	$\min \sum a_i^2$	0.02	132.82	0.06	182.01	277.6
	$\min \sum F_i$	0.08	134.62	0.28	186.17	307.91
4	$\min \sum a_i^2$	0.19	98.17	0.63	203.33	278.26
	$\min \sum F_i$	0.22	106.17	0.73	184.91	319.29